# Single-Phase Multifunctional Onboard Battery Chargers with Active Power Decoupling Capability

Hoang Vu Nguyen and Dong-Choon Lee
Department of Electrical Engineering, Yeungnam University,
280 Daehak-Ro, Gyeongsan, Gyeongbuk, 38541 Korea
E-mail: nhvu20@gmail.com, dclee@yu.ac.kr

***Abstract*—In this paper, a single-phase multifunctional onboard battery charger for electric vehicles (EVs) is proposed, where the active power decoupling capability is provided by utilizing the low voltage (LV) battery charging circuit. For this, the buck converter for the LV battery charger is used as an active power decoupling (APD) circuit while the high voltage (HV) battery is connected to the grid, by which the inherent second-order ripple power component of the single-phase charger is filtered out. Hence, small film capacitors can replace the large electrolytic capacitors, leading to the reduction of cost and the volume of the charger for EV applications. The effectiveness of the proposed charger is verified by experimental results.**

***Keywords— Active power decoupling, electric vehicles, onboard charger, single-phase chargers***

## I. INTRODUCTION

Nowadays, with the advent of more stringent regulations related to emission, global warning, and resource constraints, electric vehicles (EVs) have attracted an increasing attention from vehicle manufactures, governments, and consumers [1]–[3]. In plug-in EVs, their batteries are charged from the grid through the onboard charger by connecting to the grid. Normally, there are two usages of batteries in the EVs. One is the HV battery for traction motor drives and the other is the LV battery for auxiliary power supplies feeding the loads such as lighting and signaling circuits, entertainments, automatic seats, and other electronic devices. Instead of alternators in the conventional vehicles with an internal combustion engine, this LV battery is charged from the HV battery through the auxiliary charger system. The onboard battery chargers usually require a long life cycle, small volume and light weight [4].

In single-phase HV battery chargers, there is an inherent ripple power component that is fluctuated at double the grid frequency, which causes the DC-link voltage ripple. To smoothen this low-frequency power ripple, the large capacitors are needed. However, since the electrolytic capacitors are not preferable in automobile applications due to its short life time, they need to be replaced by the film capacitor which is reliable. For this, the ripple power should be filtered out so that small film capacitors can be employed. Recently, a number of active power decoupling circuits have been presented to reduce the ripple power at the DC-link [5]–[9]. The main idea is to use additional circuits to absorb the power ripple, which leads to the increase of the system complexity and the cost as well as the addition of losses that decreases the overall inverter efficiency. In the meanwhile, several research works have been proposed to achieve the reduction of volume and weight of the battery charger, where some switches and devices are utilized in common to minimize the circuit components [10]–[13]. However, a capacitance minimization has not been considered in these works. In [14], an integration of active power filter and LV battery charger has been introduced to reduce the overall size of the converter. However, this circuit is operated only in a unidirectional power flow. Also, the capacitor in the APD circuit is not discharged fully, which means that the capacitor is not utilized for power decoupling function.

In this paper, a multifunctional single-phase onboard battery charger is proposed, which can operate at three different modes. In the first operating mode, the HV battery is charged when the EV is connected to the power grid, where the LV battery side is isolated. The second operating mode is to supply surplus power from the HV battery to the grid, where the charger is operated as an inverter. The third operating mode is to charge the LV battery from the HV battery. In addition, the buck converter for LV battery charger circuit can be utilized as an active filter to filter the low frequency power ripple at the DC-link when the charger is operated at V2G and G2V modes. Therefore, only two small film capacitors can be employed instead of large electrolytic capacitors at the DC-link. With the proposed LV battery charger with the active power decoupling function, the size and cost of the onboard battery charger can be reduced significantly. The simulation and experimental results are verified the validity of the proposed system.

## II. PROPOSED MULTIFUNCTIONAL ONBOARD BATTERY CHARGERS

### *A. Configuration of Circuit*

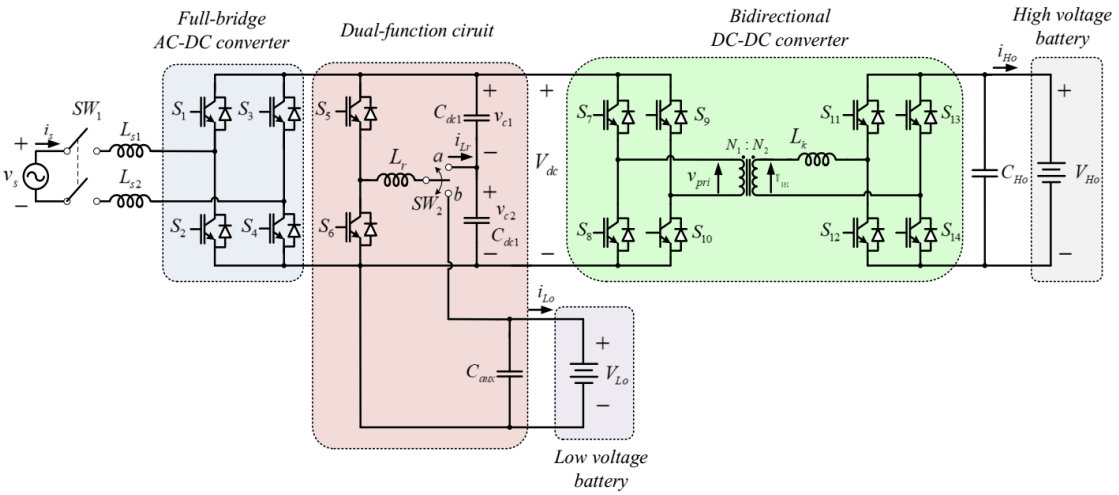


Fig. 1. Circuit configuration of the proposed multifunctional charger.

Fig. 1 shows a circuit configuration of the proposed multifunctional battery charger. The first stage is a full-bridge AC-DC converter, the second one is a dual active bridge (DAB) DC-DC converter, and the last one is a dual-functional circuit (DFC) for LV battery charging and active power decoupling.

When the $SW_1$ is closed, the system is operated in either G2V or V2G modes. So, the HV battery is charged from the gird or release power back to the grid. During this period, the DFC works as an APD circuit to absorb the inherent power ripple in the single-phase system, where small film capacitors can be used. It should be noted that the ripple power is decoupled by two identical film capacitors and an inductor. In this case, the $SW_2$ is switched to point "a", so the ripple power does not flow into the LV battery. When the $SW_1$ is open, the $SW_2$ is changed to point "b". In this period, two identical capacitors play a role in the output filter of DAB and the LV battery can be charged by the DFC from the HV battery.

### B. Proposed Dual Functional Circuit

When the $SW_2$ is connected to terminal "a" and the DFC acts as an APD circuit, two capacitors ($C_{dc1}$=$C_{dc2}$=$C_r$ ) are connected in series to build the DC link, whose midpoint is connected to the half bridge through a small inductor $L_r$ [15]. When the $SW_2$ is connected to terminal "b" and the DFC works as an LV battery charger, it is operated like the DC-DC buck converter. In this case, the DAB provides a galvanic isolation between HV battery and LV battery. Furthermore, the switching devices in this circuit can be easily integrated with the full-bridge AC-DC converter, where a three-phase IPM module can be employed, resulting in a simplified design of the system hardware.

## III. Control Method for Proposed Battery Chargers

### A. Active Power Decoupling Function

When the SW1 is closed, the vehicle is connected to the grid. In this case, the $SW_2$ is connected to terminal "a", then the DFC acts as an APC circuit. It is assumed that the input voltage and current are sinusoidal as

$$v_s = \sqrt{2}V_s \sin(\omega t) \tag{1}$$

$$i_s = \sqrt{2}I_s \sin(\omega t) \tag{2}$$

where $V_s$ and $I_s$ are the rms values of the input voltage and current, respectively, and ω is the line angular frequency. Then, the instantaneous input power, with the inductor power taken into account, is expressed as

$$p_0 = p_s - p_{Ls} = V_s I_s(1-\cos(2\omega t)) - \omega L_s I_s^2 \sin(2\omega t). \tag{3}$$

The time-varying terms on the right-hand side of (3) are the ripple component to be compensated by the half-bridge circuit. In order to achieve this, the voltages of the two capacitors should contain a fundamental component with an opposite phase each other. The upper and lower capacitor voltages can be expressed, respectively, as

$$v_{c1} = \frac{V_{dc}}{2} - \sqrt{2}V_c \cos(\omega t + \varphi) \tag{4}$$

$$v_{c2} = \frac{V_{dc}}{2} + \sqrt{2}V_c \cos(\omega t + \varphi). \tag{5}$$

where,

$$V_c = \sqrt{\frac{\sqrt{(V_s I_s)^2 + (\omega V_s I_s^2)^2}}{2\omega C_r + \omega L_r (2\omega C_r)^2}} \tag{6}$$

and

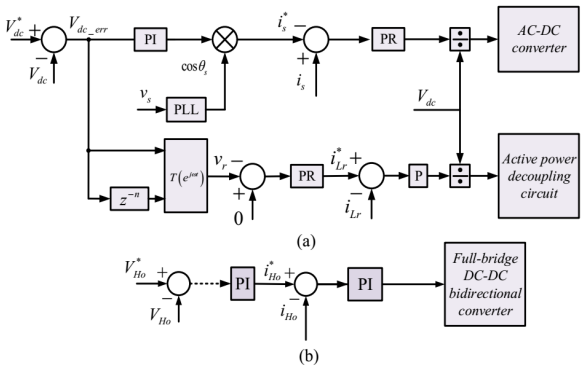


Fig. 2. Control block diagram of the proposed battery charger in G2V mode. (a) Control of AC-DC converter and APD circuit. (b) Control of HV battery in charging mode.

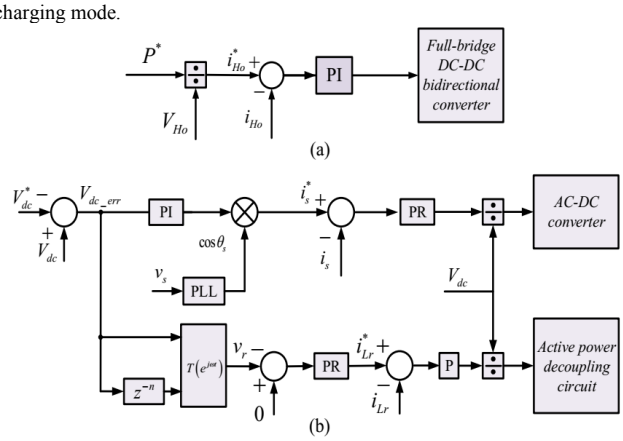


Fig. 3. Control block diagram of the proposed battery charger in V2G mode. (a) Control of HV battery in discharging mode. (b) Control of grid-connected DC-AC inverter.

$$\varphi = \frac{1}{2}\arctan\left(-\frac{V_s}{\omega V_s I_s}\right). \tag{7}$$

Then, the capacitor voltage references for active power decoupling function can be determined by (4) and (5). However, it is difficult to achieve a perfect power decoupling if there are uncertainties and disturbances in the system. Therefore, a close loop control is applied to solve this issue [15].

Fig. 2 show the control block diagram of AC-DC converter and APD circuit in G2V mode, in which the proportional-resonant (PR) controller is adopted to control the source current. For controlling the DC-link voltage, the proportional-integral (PI) controller is used. The aim of the APD circuit is to force the voltage ripple component in the DC link to be zero. The input error of DC-link voltage controller is of the second order frequency component, which needs to be transferred to a fundamental component by using the transformation matrix as

$$T(\omega t) = \begin{bmatrix} \cos(\omega t) & \sin(\omega t) \\ -\sin(\omega t) & \cos(\omega t) \end{bmatrix} \tag{8}$$

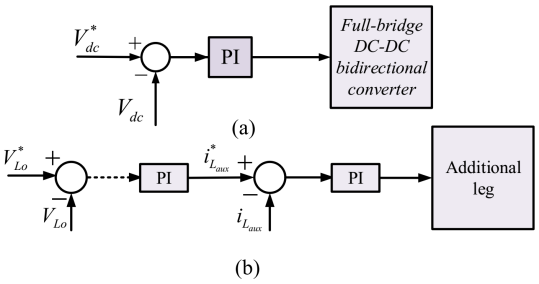


Fig. 4. Control block diagram of the proposed battery charger in HV battery to LV battery mode. (a) Control of DAB converter. (b) Control of DFC

TABLE I. PARAMETERS OF EV CHARGING SYSTEM

| Parameters | Value |
|---|---|
| HV battery power | 3.3 kW |
| LV battery power | 1 kW |
| DC output voltage | 220 V |
| Input voltage | 110 V RMS |
| $C_r$ | 200 uF |
| $L_r$ | 1.5 mH |
| Transformer turn ratio | 2:1 |
| HV battery voltage | 200 V |
| LV battery voltage | 24 V |
| $C_{aux}$ | 100 uF |
| $C_{Ho}$ | 100 uF |
| Switching frequency | 10 kHz |
| $L_{s1}$, $L_{s2}$ | 1.5 mH |
| $L_k$ | 30 uH |

In order to produce a quarter-cycle phase displacement of the second input signal for $T(\omega t)$, the number of delays, $n$, is set as $f_s/(8f)$, where $f_s$ is the sampling frequency and f is the fundamental frequency. Then, the PR controller is adopted to control the error to be zero, as shown in Fig 2(a).

The control block diagram for HV battery charging is shown in Fig. 2(b), where the PI controllers are used to control the current and voltage of the battery. The phase-shift PWM is adopted to generate the gating signal for the DAB converter.

Fig. 3 shows the control block diagram of charger in V2G mode. In this case, the DAB converter is used to control the battery current. The current reference is calculated based on the active power reference. The closed-loop control is also applied to control the APD circuit.

### *B. LV Battery Charging*

Fig. 4 shows the control block diagram of charging the LV battery from the HV battery. In this mode, the DC-link voltage is controlled by the DAB converter, where the PI controller is adopted to control the DC-link voltage, as shown in Fig. 4(a). For charging the LV battery, the CC-CV charging mode is used, as shown in Fig. 4(b).

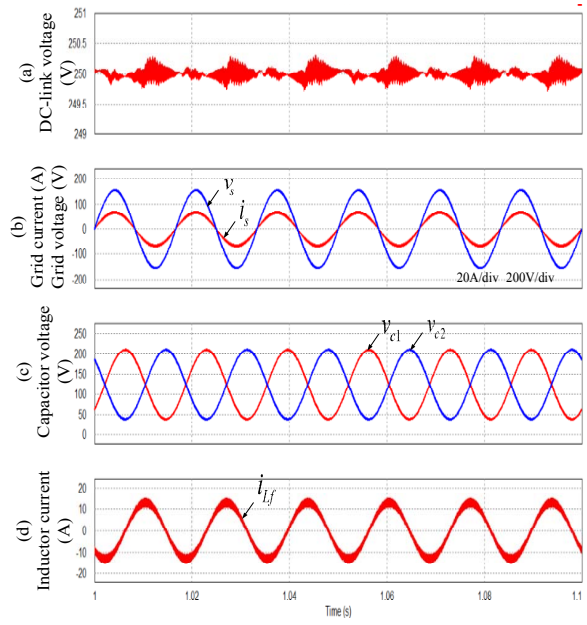


Fig. 5. Control of battery charger in G2V mode. (a) DC-link voltage. (b) Input current and input voltage. (c) Capacitor voltage. (d) Inductor current.

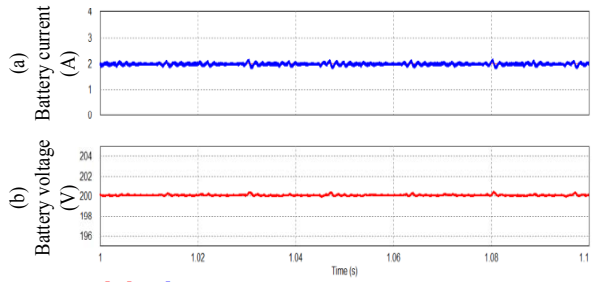


Fig. 6. Control performance of DAB DC-DC converter at constant-current charging profile. (a) Battery current. (b) Battery voltage.

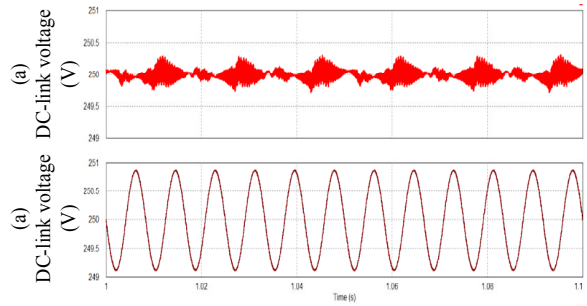


Fig. 7. Comparison of DC-link voltages in the cases of (a) 200 µF DC-link capacitor with APC circuit. (b) 3200 µF DC-link capacitor.

## IV. Simulation Results

To verify the effectiveness of the proposed circuit, the PSIM simulation has been carried out. The system parameters are listed in Table I.

Fig. 5 shows the control performance of the proposed battery charger in G2V mode, in which the hybrid converter

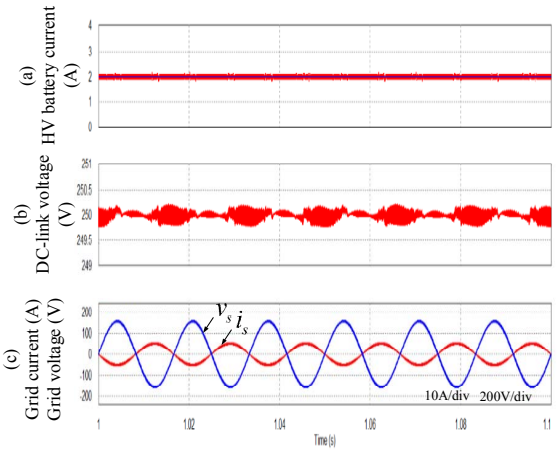


Fig. 8. Control of battery charger in V2G mode. (a) Battery current. (b) DC-link voltage. (c) Grid current and grid voltage.

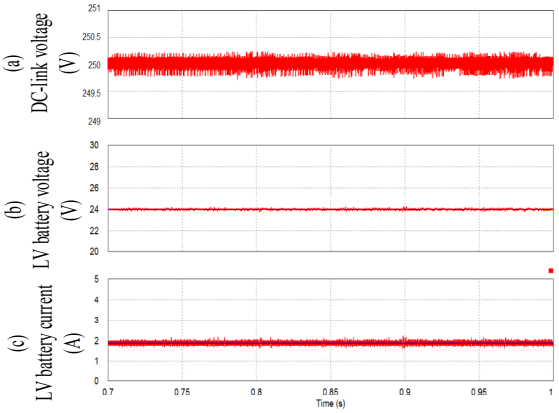


Fig. 9. Control of battery charger in H2L mode. (a) DC-link voltage. (b) LV battery voltage. (b) LV battery current.

s

works as an APC circuit. It can be seen from Fig. 5(a) that the DC-link voltage ripple is about 1% compared with the average voltage value of 250 V. The input current and voltage are shown in Fig. 5(b), where the input current is controlled to be sinusoidal at unity power factor. Fig. 5 (c) shows the upper and lower capacitor voltages with a sinusoidal waveform, which match well with the theoretical analysis. The inductor current is shown in Fig. 5(d), where its peak value is about 15A.

Fig. 6 shows the control performance of the DC-DC converter with a constant current charging condition. It can be seen that the current is regulated well at 2A and the battery voltage is 200V. Next, the comparison of DC-link voltages between the conventional method using 3200 µF capacitors and the proposed method using 200 µF capacitors with the APD circuit is shown in Fig. 7. For the conventional topology, a 3200 µF of DC-link capacitor is needed to meet the same magnitude of DC voltage ripple as in the proposed APD circuit.

The operation of the proposed charger in V2G mode is shown in Fig. 8. The battery current is regulated at 2 A, as

TABLE II. PARAMETERS OF EV CHARGING SYSTEM

| Parameters | Value |
|---|---|
| Power rating | 1 kW |
| DC-link voltage | 250 V |
| Input voltage | 110 V RMS |
| $C_r$ | 200 uF |
| $L_r$ | 1.5 mH |
| HV battery voltage | 200 V |
| $R_{Ho}$, $R_{Lo}$ | 100 Ω , 12 Ω |
| LV battery voltage | 24 V |
| $C_{aux}$ | 100 uF |
| $C_{Ho}$ | 100 uF |
| Switching frequency | 10 kHz |
| $L_{s1}$, $L_{s2}$ | 1 mH |

shown in Fig. 8(a). The DC-link voltage is controlled well with about 1% ripple as shown in Fig. 8(b). Fig. 8(c) shows the typical waveforms during V2G mode with the constant active power to the grid, where the grid current is controlled to be sinusoidal.

Fig. 9 shows the typical operating waveforms during the H2L operation mode. The DC-link voltage is adjusted well at 250 V by the DC-DC converter. The voltage and current of the LV battery are shown in Fig. 9(a) and Fig. 9(b), respectively, which are controlled well at their reference values.

## V. EXPERIMENTAL RESULTS

To verify the effectiveness of the proposed circuit, a prototype was built at the laboratory. The system parameters are listed in Table II. A 32-bit DSP chip (TMS320F28335) was used as the main controller, where the Xilinx FPGA device is employed to generate a switching frequency of 10 kHz.

Fig. 10 shows the experimental results of the proposed battery charger in G2V mode, in which the DFC works as an APC circuit. It can be seen from Fig. 10(a) that the DC-link voltage ripple is about 2%. The input current and voltage are shown in Fig. 10(b), where the input current is controlled to be sinusoidal at unity power factor. The inductor current is shown in Fig. 10(c) and its peak value is about 20A. Fig. 10(d) shows the upper and lower capacitor voltages which are sinusoidal. The LV battery current is zero since the DFC is operated for active power decoupling function, as shown in Fig. 10(e). Fig. 10(f) and (g) show the control performance of DC-DC converter at a constant-current charging condition. It can be seen that the current is well regulated at 2 A, and the battery voltage is 200 V.

The transient responses of the battery charger system are shown in Fig. 11, where the charging current is changed in steps. The DC-link voltage variations for load changes are kept below 5%.

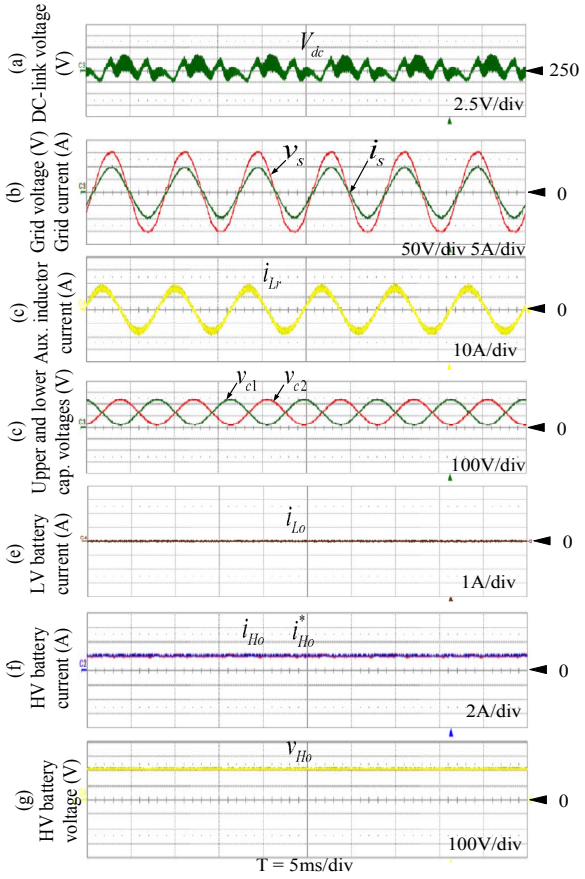


Fig. 10. Control of battery charger in V2G mode. (a) DC-link voltage. (b) Input current and voltage. (c) Inductor current. (d) Capacitor voltage. (e) LV battery current. (f) HV battery current. (g) HV battery voltage.

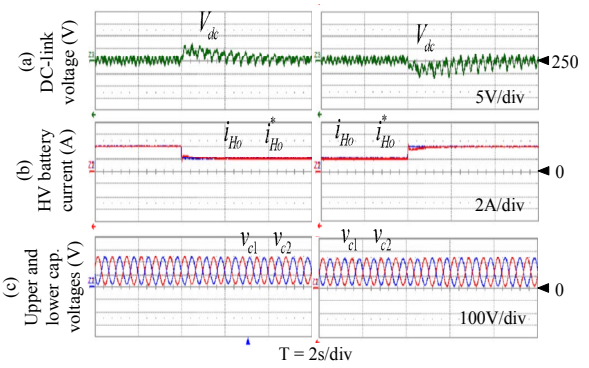


Fig. 11. Transient responses for stepwise load changes. (a) DC-link voltage. (b) HV battery current. (c) Capacitor voltage.

The operation of the proposed charger in V2G mode is shown in Fig. 12. The HV battery current is controlled by the DC-DC converter, as shown in Fig. 12(a). Fig. 12(b) shows the DC-link voltage, which is well controlled with 2% ripple components. The grid current is also controlled to be sinusoidal, as shown in Fig. 12(c).

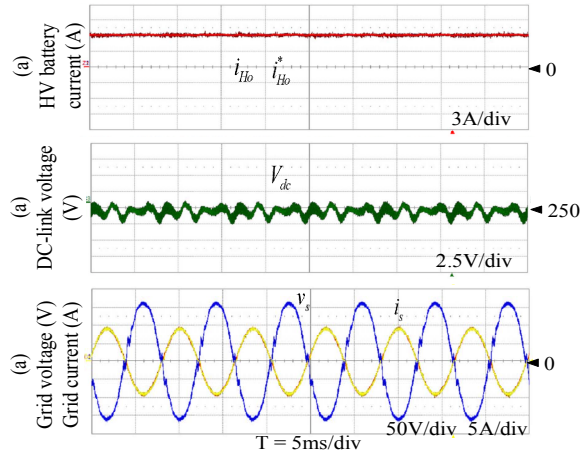


Fig. 12. Control performance of battery charger in V2G mode. (a) HV battery current. (b) DC-link voltage. (c) Input current and voltage.

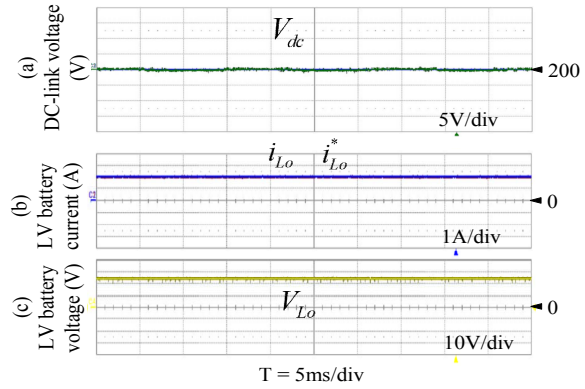


Fig. 13. Control performance of battery charger in H2L mode. (a) DC-link voltage. (b) LV battery current. (c) LV battery voltage.

Fig. 13 shows the operation of the battery charger for the H2L mode. The DC-link voltage is well controlled at 200 V as shown in Fig. 13(a). The LV battery current and voltage are shown in Fig. 13(b) and Fig. 13(c), respectively, which are well controlled at their references.

## VI. CONCLUSIONS

In this paper, a multifunction onboard battery charger for EVs with small DC-link capacitors has been proposed, which can operate in three different modes. The proposed charger system utilizes the common components for the LV battery charger and the APD circuit. Therefore, the charger can operate with APC function without additional switches, heat sink, and corresponding gate circuit, so that the small film capacitor can be used at the DC-link. The effectiveness of the proposed system has been verified by simulation and experimental results.

## ACKNOWLEDGEMENT

This research was supported by the National Research Foundation of Korea (NRF) grant funded by the Korea government (MSICT) (NRF-2017R1A2A2A05069629).

## REFERENCES

[1] C. C. Chan, A. Bouscayrol, and K. Chen, "Electric, hybrid, and fuel-cell vehicles: architectures and modeling," *IEEE Trans. Veh. Technol.*, vol. 59, no. 2, pp. 589–598, Feb. 2010.

[2] Q. Qian, W. Sun, T. Zhang, and S. Lu, "A voltage-fed single-stage PFC full-bridge converter with asymmetric phase-shifted control for battery chargers," *J. Power Electron.*, vol. 17, no. 1, pp. 31–40, 2017.

[3] M. Yilmaz and P. T. Krein, "Review of charging power levels and infrastructure for plug-in electric and hybrid vehicles," in *2012 IEEE International Electric Vehicle Conference, IEVC 2012*, 2012, vol. 28, no. 5, pp. 1–8.

[4] S. Haghbin, S. Lundmark, M. Alakula, and O. Carlson, "An isolated high-power integrated charger in electrified-vehicle applications," *IEEE Trans. Veh. Technol.*, vol. 60, no. 9, pp. 4115–4126, Nov. 2011.

[5] Y. Tang, F. Blaabjerg, and P. C. Loh, "Decoupling of fluctuating power in single-phase systems through a symmetrical half-bridge circuit," *IEEE Trans. Power Electron.*, vol. 30, no. 4, pp. 1855–1865, Mar. 2015.

[6] Y. Sun, Y. Liu, M. Su, W. Xiong, and J. Yang, "Review of active power decoupling topologies in single-phase systems," *IEEE Trans. Power Electron.*, vol. 31, no. 7, pp. 4778–4794, 2016.

[7] R. Chen, Y. Liu, and F. Z. Peng, "DC capacitor-less inverter for single-phase power conversion with minimum voltage and current stress," *IEEE Trans. Power Electron.*, vol. 30, no. 10, pp. 5499–5507, Oct. 2015.

[8] M. A. Vitorino, R. Wang, M. B. de R. Correa, and D. Boroyevich, "Compensation of DC-link oscillation in single-phase-to-single-phase VSC/CSC and power density comparison," *IEEE Trans. Ind. Appl.*, vol. 50, no. 3, pp. 2021–2028, May 2014.

[9] H. V. Nguyen, Y.-C. Jeung, and D.-C. Lee, "Battery charger with small DC-link capacitors for G2V applications," in *2016 IEEE International Conference on Sustainable Energy Technologies (ICSET)*, 2016, pp. 315–319.

[10] Young-Joo Lee, A. Khaligh, and A. Emadi, "Advanced integrated bidirectional AC/DC and DC/DC converter for plug-in hybrid electric vehicles," *IEEE Trans. Veh. Technol.*, vol. 58, no. 8, pp. 3970–3980, Oct. 2009.

[11] S. Dusmez and A. Khaligh, "A compact and integrated multifunctional power electronic interface for plug-in electric vehicles," *IEEE Trans. Power Electron.*, vol. 28, no. 12, pp. 5690–5701, Dec. 2013.

[12] S. Kim and F. Kang, "Multi-functional on-board battery charger for plug-in electric vehicles," *IEEE Trans. Ind. Electron.*, vol. 62, no. 6, pp. 1–1, 2014.

[13] J. G. Pinto, V. Monteiro, H. Gonçalves, and J. L. Afonso, "Onboard reconfigurable battery charger for electric vehicles with traction-to-auxiliary mode," *IEEE Trans. Veh. Technol.*, vol. 63, no. 3, pp. 1104–1116, 2014.

[14] R. Hou and A. Emadi, "Applied integrated active filter auxiliary power module for electrified vehicles with single-phase onboard chargers," *IEEE Trans. Power Electron.*, vol. 32, no. 3, pp. 1860–1871, Mar. 2017.

[15] Y. Tang, Z. Qin, F. Blaabjerg, and P. C. Loh, "A dual voltage control strategy for single-phase PWM converters with power decoupling function," *IEEE Trans. Power Electron.*, vol. 30, no. 12, pp. 7060–7071, Dec. 2015.